The Observed Structure of Convectively Coupled Kelvin Waves: Comparison with Simple Models of Coupled Wave Instability

KATHERINE H. STRAUB

Cooperative Institute for Research in the Environmental Sciences, University of Colorado, and NOAA Aeronomy Laboratory, Boulder, and Department of Atmospheric Science, Colorado State University, Fort Collins, Colorado

GEORGE N. KILADIS

NOAA Aeronomy Laboratory, Boulder, Colorado

(Manuscript received 24 June 2002, in final form 18 December 2002)

ABSTRACT

Observations of the horizontal and vertical structure of convectively coupled Kelvin waves are presented and are compared with the predicted structures of moist Kelvin (or gravity) waves in three simple models of coupled wave instability: wave–conditional instability of the second kind (CISK), wind-induced surface heat exchange (WISHE), and stratiform instability. The observations are based on a linear regression analysis of multiple years of ECMWF reanalysis and station radiosonde data. Results suggest that both the wave-CISK and stratiform instability theories successfully predict many important features of observed moist Kelvin waves, but that unrealistic aspects of these models limit their ability to provide comprehensive explanations for the dynamics of these waves. It is suggested that an essential component of any theory for moist Kelvin waves is the second baroclinic mode heat source associated with stratiform precipitation.

1. Introduction

Observations by Takayabu (1994), Pires et al. (1997), Wheeler and Kiladis (1999, hereafter WK99), and Wheeler et al. (2000, hereafter WKW00) demonstrate the existence of large-scale, zonally propagating variations in tropical cloudiness that are dynamically coupled to equatorially trapped wave structures in the troposphere and lower stratosphere. Space–time spectra of deep convective cloudiness data reveal spectral peaks that lie along the dispersion curves for the equatorially trapped shallow water waves discussed by Matsuno (1966), such as Kelvin, $n = 1$ equatorial Rossby, mixed Rossby–gravity, and inertio-gravity waves. The observed spectral peaks correspond to equatorial waves with relatively small implied equivalent depths, typically 10–100 m, consistent with the fact that these convectively coupled, or moist, equatorial waves propagate at phase speeds much slower than their dry counterparts. For example, convectively coupled Kelvin waves are observed to propagate eastward at 15–20 m s^{-1}, whereas dry Kelvin waves in the lower stratosphere propagate at speeds of 30–40 m s^{-1} (WKW00). Presumably, the reduction in phase speed from dry to moist wave involves the interaction between tropical convection and the large-scale dynamical structure of the waves. The precise nature of this interaction, however, is not yet fully understood.

Several theories have been proposed to explain the existence of convectively coupled equatorial waves and the dynamics governing their behavior, including wave–conditional instability of the second kind (CISK; Hayashi 1970; Lindzen 1974), wind-induced surface heat exchange (WISHE; Emanuel 1987; Neelin et al. 1987; Yano and Emanuel 1991), and more recently, stratiform instability (Mapes 2000; Majda and Shefter 2001).[1] While all of these theories predict the existence of convectively coupled wave instabilities of some form, the true test of each lies in its ability to reproduce the observed structures of convectively coupled waves. However, there are few observational studies available presently with which to compare model results. An important step in improving our understanding of convectively coupled waves thus lies in an accurate observational diagnosis of the structures and phase relationships in these waves.

The present study provides detailed observations of one particular type of convectively coupled equatorial

Corresponding author address: Dr. Katherine H. Straub, Dept. of Geological and Environmental Sciences, Susquehanna University, 514 University Avenue, Selinsgrove, PA 17870.
E-mail: straubk@susqu.edu

[1] A more complete listing of theories relevant to convective coupling can be found in Raymond and Torres (1998).

wave: the Kelvin wave. Convectively coupled Kelvin waves are one of the dynamically simplest classes of equatorially trapped waves, since their structure near the equator is essentially that of an eastward-propagating gravity wave. Observations of convectively coupled Kelvin waves may therefore provide a basis upon which theories of convectively coupled gravity waves, derived in relatively simple nonrotating two-dimensional frameworks, may be tested. Once a theory has successfully reproduced the observations in this simple case, it can be expanded to include rotation and other dynamical interactions. It may then become possible to understand the more complex three-dimensional structures of observed convectively coupled Kelvin, mixed Rossby–gravity, and $n = 1$ equatorial Rossby waves (WKW00), as well as the Madden–Julian oscillation (MJO; Madden and Julian 1994). The observed structures of convectively coupled Kelvin waves thus provide a simple test case through which the interaction between tropical deep convection and atmospheric wave circulations can initially be studied.

The observations presented in this study emphasize the tropospheric structure of convectively coupled Kelvin waves. The lower-stratospheric structure of Kelvin and other equatorially trapped waves has been explained by WKW00 in terms of upward-propagating dry waves forced by a tropospheric heat source with a vertical structure similar to observations (see also Andrews et al. 1987). The tropospheric structure, on the other hand, is not as easily understood through these dry vertically propagating wave arguments. The approach taken here relies on ''vertical mode'' thinking rather than ''vertically propagating wave'' thinking, as has been similarly applied in observational and modeling studies such as Mapes (1993), Haertel and Johnson (1998), Mapes (2000), and Majda and Shefter (2001).

The remainder of this paper is organized as follows. In section 2, theories and models of convective coupling in equatorial waves are described in more detail. The datasets and methodology used in analyzing observed convectively coupled Kelvin waves in the present study are described in section 3. In section 4, the horizontal and vertical structures of Kelvin waves in the equatorial Pacific are presented, based on global reanalysis datasets, and are compared with radiosonde observations. Finally, in section 5, a discussion of these observations in the context of the theories described in section 2 is presented.

2. Theories of coupled wave instability

The interaction between deep convection and large-scale wave circulations in the tropical atmosphere has remained a subject of discussion for many years. At present, no theory is generally accepted as both 1) providing a complete conceptual picture of this interaction and 2) capable of reproducing observed features through numerical simulations based on such conceptualizations. Several proposed theories will be introduced and discussed in this section, and compared with observations in section 5.

a. Wave-CISK

One of the first widely known theories describing the interaction between convection and the large-scale circulation in the Tropics is CISK. A broad interpretation of CISK theory states that instabilities in the large-scale circulation can be driven by the cooperative interaction between small-scale convective heating and the large-scale circulation [see Stevens et al. (1997) for other interpretations of CISK]. Namely, if deep convection is excited in a region of large-scale, low-level convergence, its associated latent heating will induce dynamical circulations that promote additional large-scale convergence (via a column-integrated warm anomaly), leading to more deep convection and further heating. When the initial large-scale convergence is supplied by a wave, the theory is known as wave-CISK (Hayashi 1970; Lindzen 1974). A schematic diagram of a first baroclinic Kelvin mode amplifying through the wave-CISK mechanism is presented in Fig. 1a. A positive correlation between latent heating (i.e., deep convection) and warm temperatures in the wave generates eddy available potential energy (EAPE), which induces wave growth. Observations of equatorial waves that display a positive correlation between heating and temperature are provided in studies such as Reed and Recker (1971), Yanai et al. (1973, 2000), Stevens et al. (1997), Haertel and Johnson (1998), and WKW00.

Although wave-CISK remains a reasonable conceptual picture of certain wavelike convection–circulation interactions in the Tropics, linear stability analyses based on various wave-CISK parameterizations have not yet been able to avoid the ''ultraviolet catastrophe,'' in which growth rates are largest on the smallest resolvable scales (Crum and Dunkerton 1992; Matthews and Lander 1999). Despite these numerical difficulties, modeled wave-CISK modes do provide simple structures with which to compare observations. Typically, the unstable modes produced in wave-CISK simulations propagate at phase speeds between 15–30 m s^{-1} (e.g., Wang 1988; Matthews and Lander 1999), similar to the convectively coupled Kelvin waves described in this study, which propagate eastward at 15–20 m s^{-1}. The structure of modeled Kelvin wave-CISK modes will be discussed in relation to observed Kelvin wave structures in section 5a.

The mechanism for the reduction in phase speed in wave-CISK-driven Kelvin waves involves an interaction between multiple vertical modes (Lau and Peng 1987; Chang and Lim 1988; Matthews and Lander 1999). A slower mode, with a higher vertical wavenumber, provides stronger boundary layer convergence and controls the speed of the wave. A faster, lower wavenumber mode dominates the vertical structure of the

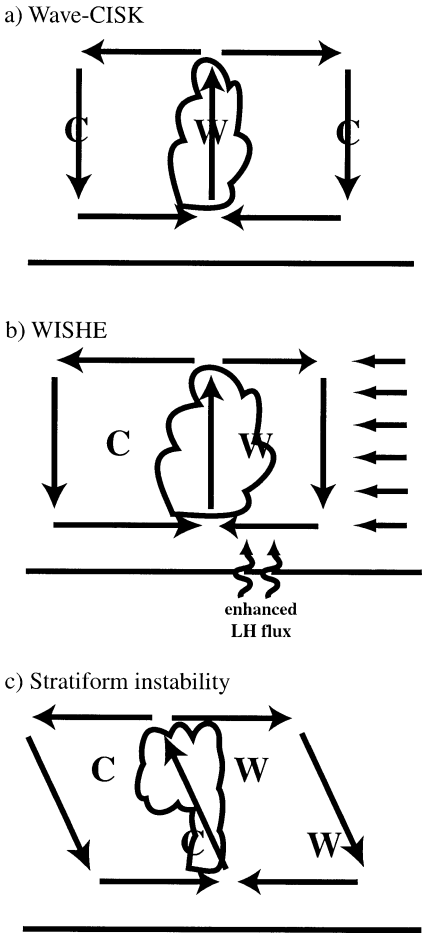

FIG. 1. Schematic longitude–height diagrams illustrating the (a) wave-CISK, (b) WISHE, and (c) stratiform instability mechanisms of wave amplification for a first baroclinic mode Kelvin wave. Vectors represent anomalous winds [except for vectors at right in (b), which represent easterly basic-state winds], and cloud illustrations represent populations of cloud systems of the indicated type (convective or stratiform). The letter W (C) represents warm (cold) anomalies. Upward arrows crossing the lower boundary represent surface fluxes.

wave (Matthews and Lander 1999). Convectively coupled Kelvin waves with phase speeds of 15–30 m s^{-1} are produced in wave-CISK simulations when heating maximizes in the upper troposphere, as observed.

b. WISHE

An alternative theory to explain the existence of convectively coupled waves is WISHE (Emanuel 1987; Neelin et al. 1987; Yano and Emanuel 1991). WISHE instabilities arise through the interaction between surface heat fluxes and a wave's dynamical fields. The application of WISHE theory to equatorial waves was introduced in the context of quasi-equilibrium (QE) theory (Arakawa and Schubert 1974). The QE closure implies that the convective available potential energy (CAPE) generated by adiabatic cooling and low-level moisture convergence in the rising branch of a large-scale wave circulation will be quickly consumed by convection, such that the cooling is nearly balanced by latent heating (Emanuel et al. 1994). Observations are generally consistent with QE theory, since the actual temperature changes associated with strong upward motion and large convective heating rates in equatorial waves are very small compared to the values that might be expected if convection were not present (Stevens et al. 1997).

A strict application of QE theory states that convective heating will be exactly in phase with large-scale upward motion in an equatorial wave, since there is no time lag between upward motion and convective heating (Emanuel et al. 1994). A first baroclinic mode Kelvin wave propagating eastward in a strict QE system will display temperature and heating fields that are exactly in quadrature, with warm temperatures leading the upward motion and convective heating by a quarter cycle. In this system, moist unstable waves cannot grow through the interaction between convection and circulation alone, since the temperature and heating fields are always in quadrature. Emanuel et al. (1994) argue that large-scale coupled waves can thus only be neutral (i.e., neither amplifying nor decaying), or ''moist convectively damped,'' if convection slightly lags vertical motion and the heating is shifted toward the cold temperature anomaly.

WISHE theory provides a mechanism by which amplifying convectively coupled wave modes can be generated in the strict QE system by incorporating the effects of surface heat fluxes. The role of convection in WISHE is not to act as a heat source, as in wave-CISK, but instead to rapidly redistribute boundary layer moist entropy changes (e.g., as measured by equivalent potential temperature) throughout the vertical column, leading to column temperature changes. Boundary layer moist entropy fluctuations can be induced either by convection itself, in the form of convective downdrafts, or by interactions with the surface, through wind speed–dependent latent heat fluxes from the ocean (Emanuel et al. 1994). A first baroclinic mode Kelvin wave can thus amplify in the WISHE system in the presence of mean surface easterly winds, since the surface fluxes will be larger ahead of the rising branch of the wave (Fig. 1b). Convection will redistribute this increase in surface entropy throughout the troposphere, such that heating will be partially shifted into the warm phase of the wave, generating EAPE through the positive correlation between heating and temperature.

A weakness in linear WISHE theory is its assumption of nonzero basic-state winds, specifically basic-state easterlies for the case of eastward-propagating waves such as Kelvin waves and the MJO. Although surface winds in the Tropics are generally easterly over the Pacific, monsoon westerlies exist in the Indian Ocean region during both austral and boreal summer, and can extend eastward into the Pacific during strong El Niño–Southern Oscillation (ENSO) events. WISHE theory

cannot explain the intensification of eastward-propagating waves during periods of surface westerlies, or at times when the total surface fluxes are stronger to the west of the convection rather than to its east. Examples of such instances were observed during the TOGA COARE period, when an MJO propagated eastward in the western Pacific during a period of basic-state surface westerlies, and surface fluxes were strongest to the west of the deepest convection (Lin and Johnson 1996; Yanai et al. 2000).

The reduced phase speed of WISHE modes, and of QE-type closures in general, as compared to the dry speeds of uncoupled modes, is attributed to a reduction in static stability throughout the convecting column, and its effect on the wave dispersion relationship (e.g., Neelin and Held 1987; Emanuel et al. 1994). Negative moist entropy fluctuations in the boundary layer induced by convective downdrafts are redistributed throughout the column such that the greatest cooling occurs at upper levels, thus reducing the static stability of the column. The ''effective'' static stability is argued by Emanuel et al. (1994) to be approximately one-tenth the value of the dry static stability.

c. Stratiform instability

The increasing number of direct observations of tropical convection in recent years has led to new ideas about how convection is triggered, how it is organized on the mesoscale, and how these mesoscale features evolve in time. Observations by Rickenbach and Rutledge (1998) suggest that approximately 80% of rainfall in the western Pacific warm pool region may be associated with organized, mesoscale precipitation regions, of which 30%–40% falls as stratiform precipitation. Such observations suggest the important role of stratiform precipitation in the large-scale moisture, momentum, and thermodynamic budgets of the tropical atmosphere. Stratiform regions are generally more horizontally extensive than the convective regions that precede them; they also persist for long time periods after convection has dissipated, and thus may have a large impact on the potential for subsequent convective outbreaks (Houze 1997).

Two recent modeling studies, by Mapes (2000) and Majda and Shefter (2001), propose that the effects of stratiform precipitation are essential to the existence and structure of convectively coupled gravity or Kelvin waves. A ''stratiform instability'' mechanism of coupled wave instability is developed in the context of dynamically simple mode formulations that include only two vertical modes: a first baroclinic ''convective'' mode and a second baroclinic ''stratiform'' mode.

The stratiform instability mode is generated through a positive correlation between a second mode temperature wave and the second mode stratiform heating profile. In the Mapes (2000) formulation, large-scale convectively coupled gravity waves organize from initial random noise when fluctuations in the convective inhibition (CIN) are parameterized to be dominant over fluctuations in CAPE. The second mode instability is activated when deep convection is triggered by a reduction in CIN, via a second mode warm over cold temperature anomaly, and is followed at lag by a stratiform (second mode) heating over cooling profile. The lower-tropospheric cooling then further decreases CIN, which reinitializes deep convection, leading to further stratiform heating and a positive correlation between the second mode heating and temperature profiles. Figure 1c illustrates the phase relationships between convective and stratiform heating and temperature for the stratiform instability mechanism of wave amplification. Circulation and temperature anomalies tilt westward with height, and temperature anomalies have a strong second baroclinic mode structure. No particular basic-state flow is required for this mode to exist.

Stratiform instability waves propagate at phase speeds near the dry wave speed of the second internal mode (Mapes 2000). The reduction in phase speed in stratiform waves is attributed to the effects of the second vertical mode, as in wave-CISK, rather than the effect of moisture on the first vertical mode, as in WISHE (Mapes 2000; Majda and Shefter 2001).

3. Data and methodology

The observed relationships between tropical convection and the kinematic, thermodynamic, and moisture fields in convectively coupled Kelvin waves will be presented in section 4. These relationships are analyzed through the use of a linear regression technique applied to many years of data, as in previous studies (WKW00; Straub and Kiladis 2002, hereafter SK02; Straub and Kiladis 2003, hereafter SK03). Deep tropical convection associated with convectively coupled Kelvin waves is isolated using a filtered version of the 2.5°-resolution National Oceanic and Atmospheric Administration (NOAA) outgoing longwave radiation (OLR) dataset (Liebmann and Smith 1996). As described in detail in WK99 and WKW00, OLR fluctuations associated with convectively coupled Kelvin waves are separated from the raw OLR data by filtering the data in wavenumber–frequency space such that only fluctuations in the region of the climatological Kelvin wave OLR spectral peak are retained. The Kelvin wave filter retains OLR variability with periods between 2.5 and 17 days, and eastward phase speeds of 8–30 m s^{-1} (see Fig. 1 in SK02). As in SK02 and SK03, both the symmetric and antisymmetric components of OLR with respect to the equator are allowed to pass through the filter. Data have been averaged to daily temporal resolution from twice-daily resolution.

European Centre for Medium-Range Weather Forecasts (ECMWF) reanalysis data are used to represent the global atmospheric circulation. The reanalysis data are available on the same 2.5° grid as the OLR data, at

16 pressure levels between 1000 and 10 hPa, for the years 1979–93. Data are averaged to daily resolution from four-times-daily resolution. Temperature, horizontal wind, vertical motion, geopotential height, and specific humidity data at all grid points are linearly regressed at lag against the Kelvin wave–filtered OLR extracted at specific grid points of interest. The resulting regressed fields are then scaled to a -40 W m^{-2} anomaly in Kelvin wave OLR, which represents a strong Kelvin wave event.

Composites have also been calculated based on both negative and positive OLR perturbations at the same base points as used in the linear regressions. The composite results are very similar to those calculated in the regressions, for both positive and negative OLR anomalies, suggesting a strong linearity in the Kelvin wave dynamical fields and justifying the use of the linear regression technique.

Radiosonde data from the National Climatic Data Center's (NCDC) Comprehensive Aerological Reference Data Set (CARDS) are also utilized in this study to provide a validation of the reanalysis-based results. Data were extracted at either 15 mandatory levels or 29 mandatory and significant levels, depending on data resolution. The data have been averaged to daily temporal resolution and extend from 1979–99. The radiosonde data are subjected to the same linear regression procedure as the reanalysis data, based on the Kelvin wave–filtered OLR at the nearest grid point to each radiosonde station.

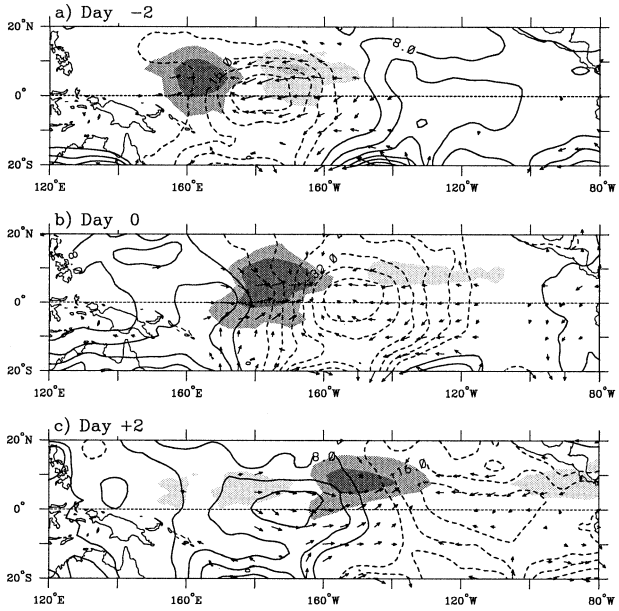

FIG. 2. Regressed OLR (shading, at ±10 and 20 W m^{-2}, dark shading negative) and ECMWF reanalysis 1000-hPa geopotential height (contours, 8 m) and winds (vectors, longest vectors 3 m s^{-1}) for days (a) -2, (b) 0, and (c) $+2$, based on a -40 W m^{-2} anomaly in Kelvin wave–filtered OLR on day 0 at the base point 7.5°N, 172.5°W. Wind vectors are plotted only where significant at the 95% level or greater.

4. Observed Kelvin wave structure

The Kelvin wave observations presented in this section are based on regressions of ECMWF reanalysis data and total OLR against the Kelvin wave–filtered OLR at the point 7.5°N, 172.5°W, in the central Pacific. This base point is the location of the maximum climatological Kelvin wave OLR variance during the boreal summer season [June–July–August (JJA)], as illustrated in SK02 and SK03, and lies along the axis of the boreal summer climatological intertropical convergence zone (ITCZ). The regressions are calculated over the 15 JJA periods from 1979–93. The results can thus be considered to be typical of Kelvin waves in the central Pacific during boreal summer. In section 4d, the reanalysis regressions are compared with regressions based on radiosonde data from Majuro, Marshall Islands, in the central Pacific.

Reanalysis- and radiosonde-based regressions have also been calculated for base points over equatorial Africa during boreal spring [March–April–May (MAM)] and in the Indian Ocean region during JJA, both of which represent local Kelvin wave OLR variance maxima. These results are not presented here, however, as the structures are similar to those in the central Pacific. The boreal summer central Pacific case is presented because the annual maximum in Kelvin wave activity occurs in this location and at this time of year, and the open ocean location of the central Pacific eliminates complications due to land effects.

a. Horizontal structure

Figure 2 illustrates the regressed horizontal structure of OLR (shading) and reanalysis 1000-hPa geopotential height (contours) and winds (vectors) for a Kelvin wave in the central Pacific, on days -2, 0, and $+2$. The OLR anomalies move eastward at approximately 17 m s^{-1}, maximizing to the north of the equator at the latitude of the climatological ITCZ, where sea surface temperatures (SSTs) are highest during boreal summer. Easterly anomalies exist to the east of the low OLR signal, while westerly anomalies exist both within the region of lowest OLR and to its west. Low (high) geopotential height anomalies maximize to the east (west) of the lowest OLR, and are symmetric with respect to the equator throughout the life cycle of the Kelvin wave. As discussed in SK02, the observed Kelvin wave dynamical fields throughout the troposphere and lower stratosphere are primarily symmetric with respect to the equator, while the OLR signal maximizes in the Northern Hemisphere in the central and eastern Pacific. The phasing of OLR, wind, and height anomalies shown in Fig. 2 for the central Pacific Kelvin wave is similar to that for Kelvin waves over Africa and the Indian Ocean (not shown). In these other locations, however, the OLR signal maximizes on the equator, due to the fact that the

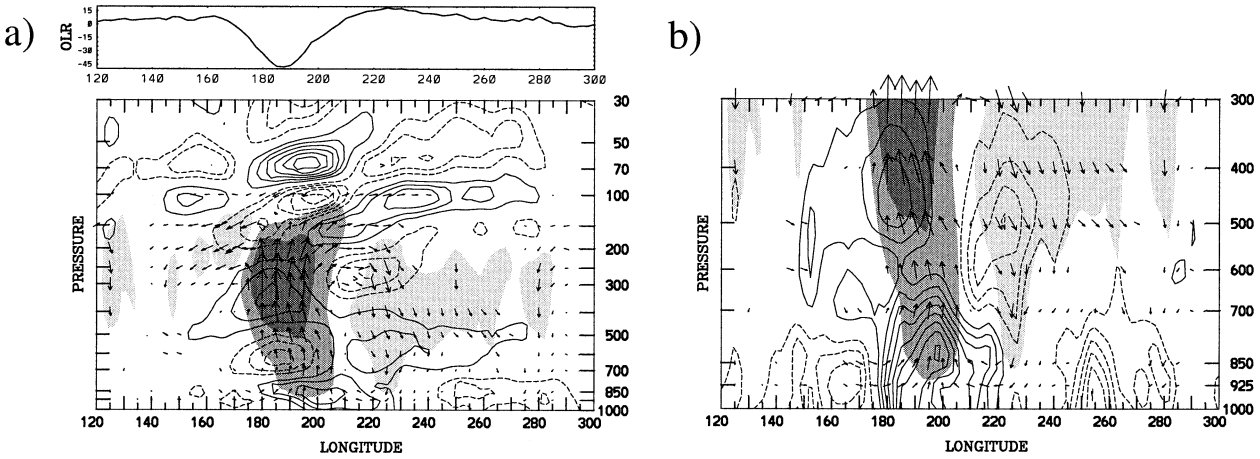

FIG. 3. (a) Longitude–height cross section along 7.5°N of regressed temperature (contours, interval 0.1 K), vertical motion (shading, at 0.2 and 0.6 cm s^{-1}), and zonal–vertical circulation (vectors). OLR cross section at 7.5°N shown above. The vertical component of the vectors has been multiplied by 700 to account for the small aspect ratio of the plot. The longest vectors represent winds of 5.0 m s^{-1}. (b) Same as (a), except for specific humidity (contours, interval 0.075 g kg^{-1}) shown only to 300 hPa.

lower boundary conditions are more symmetric with respect to the equator.

The eastward-propagating region of low OLR in Fig. 2 represents an envelope of enhanced deep cloudiness, which was shown by SK02 to primarily consist of smaller spatial scale, shorter timescale convective activity. Much of this activity is organized into westward-propagating mesoscale systems of horizontal scale 100–500 km, which include both convective and stratiform precipitation regions. It is important to recognize that the large-scale dynamical structures illustrated in this study represent the net effect of these numerous smaller-scale events that occur within the eastward-propagating cloudiness envelope.

The maximum convergence of 1000-hPa wind anomalies lies approximately 10°–15° of longitude, or approximately one-eighth of a cycle, to the east of the low OLR anomaly (not shown; see Fig. 7 of SK03). The maximum upper-tropospheric divergence is located at approximately 150 hPa, and is collocated with the OLR minimum (not shown). These relationships suggest the presence of a tilted structure in the vertical, with maximum lower-tropospheric convergence located ahead of, and upper-tropospheric divergence collocated with, the deepest convection. These relationships are further addressed in the following section.

b. Vertical structure

The vertical structure of temperature and winds associated with the Kelvin wave on day 0 is shown in Fig. 3a, a longitude–height cross section along 7.5°N (see also Fig. 8c in SK03). OLR perturbations are largest at 7.5°N on day 0 (as determined by the choice of base point), and thus the dynamical anomalies should be most directly coupled to the convection at this latitude. Although the reanalysis temperature and vertical motion fields are highly constrained by the model's convective parameterization scheme, comparisons with radiosonde data in section 4d show that the large-scale temperature structures are similar.

Figure 3a illustrates the regressed ECMWF temperature (contours), vertical motion (shading), and zonal–vertical circulation (vectors), as well as the regressed OLR (top), along 7.5°N on day 0. The strongest vertical motion anomalies are found in the upper troposphere between 180°–200°E, and are collocated with the lowest OLR. These large-scale, low-amplitude (order mm s^{-1}) vertical motion anomalies represent an average over the numerous smaller-scale, higher-amplitude convective updrafts within the eastward-propagating envelope of convection. Downward motion anomalies are weaker, more horizontally extensive, and are located primarily to the east of the low OLR on day 0. The zonal component of the low-level convergence and upper-level divergence signals can be seen in the vector winds of Fig. 3a, with low-level convergence and upward motion leading the low OLR and upper-tropospheric upward motion by approximately 15° of longitude. Upper-tropospheric divergence is located directly above the maximum upward motion. Outflow between 100 and 200 hPa spreads both east and west in the upper troposphere, but the sinking motion that completes the zonal–vertical circulation cell is stronger to the east on day 0.

The observed tropospheric temperature anomalies have much in common with previous studies of tropical convective events (e.g., Sherwood and Wahrlich 1999). These temperature anomalies project strongly onto a second baroclinic mode structure, with warm over cold anomalies in the region of large-scale upward motion and low OLR, and cold over warm anomalies to the east. The existence of a second baroclinic mode temperature structure in the troposphere, with a node at approximately 500 hPa, suggests that stratiform precip-

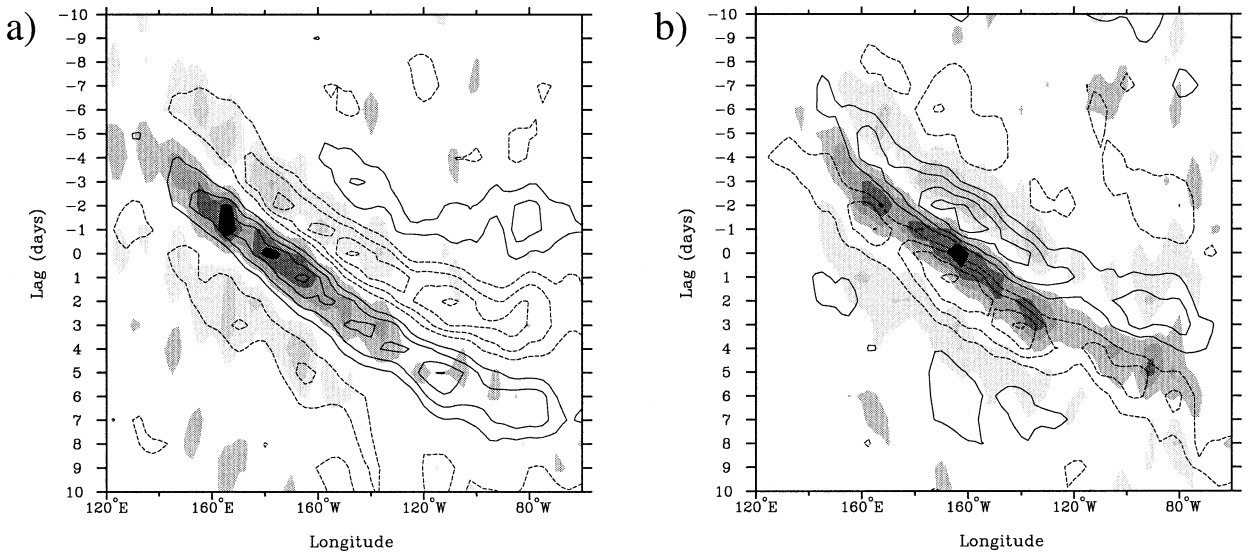

FIG. 4. Time–longitude plots of vertical motion (shading, dark negative) and temperature (contours, solid positive, contour interval 0.075 K, zero contour omitted), averaged from 0°–10°N, at (a) 300 hPa, and (b) 700 hPa. Shading in (a) is at ± 0.2 cm s^{-1} intervals and in (b) is at ± 0.075 cm s^{-1} intervals.

itation processes play a role in determining the large-scale wave structure. It is well known that regions of stratiform precipitation are marked by an overall signature of latent heating and rising motion above 500 hPa, and evaporative cooling and sinking motion below 500 hPa (Houze 1997). In a case study of a convectively coupled Kelvin wave presented in SK02, stratiform precipitation is shown to comprise greater than 50% of the total precipitating echo area throughout the wave's passage.

The observed tropospheric temperature structure in Fig. 3a is not purely second mode, however. Additional low-level temperature perturbations are seen between approximately 750 and 1000 hPa. Warm low-level air slightly leads low-level convergence and upward motion anomalies (Fig. 3a), as well as positive specific humidity perturbations (Fig. 3b). Throughout the evolution of the wave, an in-phase relationship persists between temperature, moisture, upward motion, and convergence anomalies in the 850–1000-hPa layer (not shown). These signals are consistent with the presence of enhanced shallow convection to the east of deep convection. The upward transport of moisture due to deep convection can be detected in the upper-tropospheric moist anomalies between 300 and 600 hPa in Fig. 3b, which lag the strongest upper-tropospheric upward motion anomalies and low OLR. This evolution is typically seen in studies of tropical convective disturbances (e.g., Reed and Recker 1971; Yanai et al. 1973; Sherwood and Wahrlich 1999).

A case study of a Kelvin wave in the eastern Pacific by SK02 supports the idea that on the large-scale, shallow convection tends to precede deep convection and stratiform precipitation in the Kelvin wave as it propagates eastward. Similar conclusions were reached by Xu and Randall (2001) for easterly waves in the Atlantic, with deep convection preceding stratiform precipitation by 12–24 h in these westward-propagating disturbances.

c. *Phase relationships between temperature and vertical motion*

The temperature anomalies in the layer between approximately 200–500 hPa are highly correlated with vertical motion anomalies throughout the Kelvin wave's life cycle. Shown in Fig. 4a is a time–longitude diagram of regressed 300-hPa vertical motion (shading) and temperature (contours), averaged from 0°–10°N. These two fields are also strongly correlated with OLR and 150-hPa divergence (not shown), such that upper-tropospheric warm anomalies, upward motion, 150-hPa divergence, and low OLR are all spatially and temporally phase-locked. These relationships suggest a generation of EAPE by the Kelvin wave, through the positive correlation between temperature and heating (as inferred by upward motion and low OLR). The correlation between heating, upward motion, and 150-hPa divergence also suggests a strong conversion of EAPE to eddy kinetic energy (EKE).

Similar temperature structures and phase relationships with respect to heating and OLR are shown by Haertel and Johnson (1998) for 2-day waves in the Pacific, and by Xu and Randall (2001) for easterly waves in the Atlantic. WKW00, however, found a distinct lead in warm upper-tropospheric temperature with respect to vertical motion and OLR for Kelvin waves in the Indian Ocean region, similar to that observed in the MJO, where upper-tropospheric warm temperatures lead low OLR by a quarter cycle (Hendon and Salby 1994; Yanai

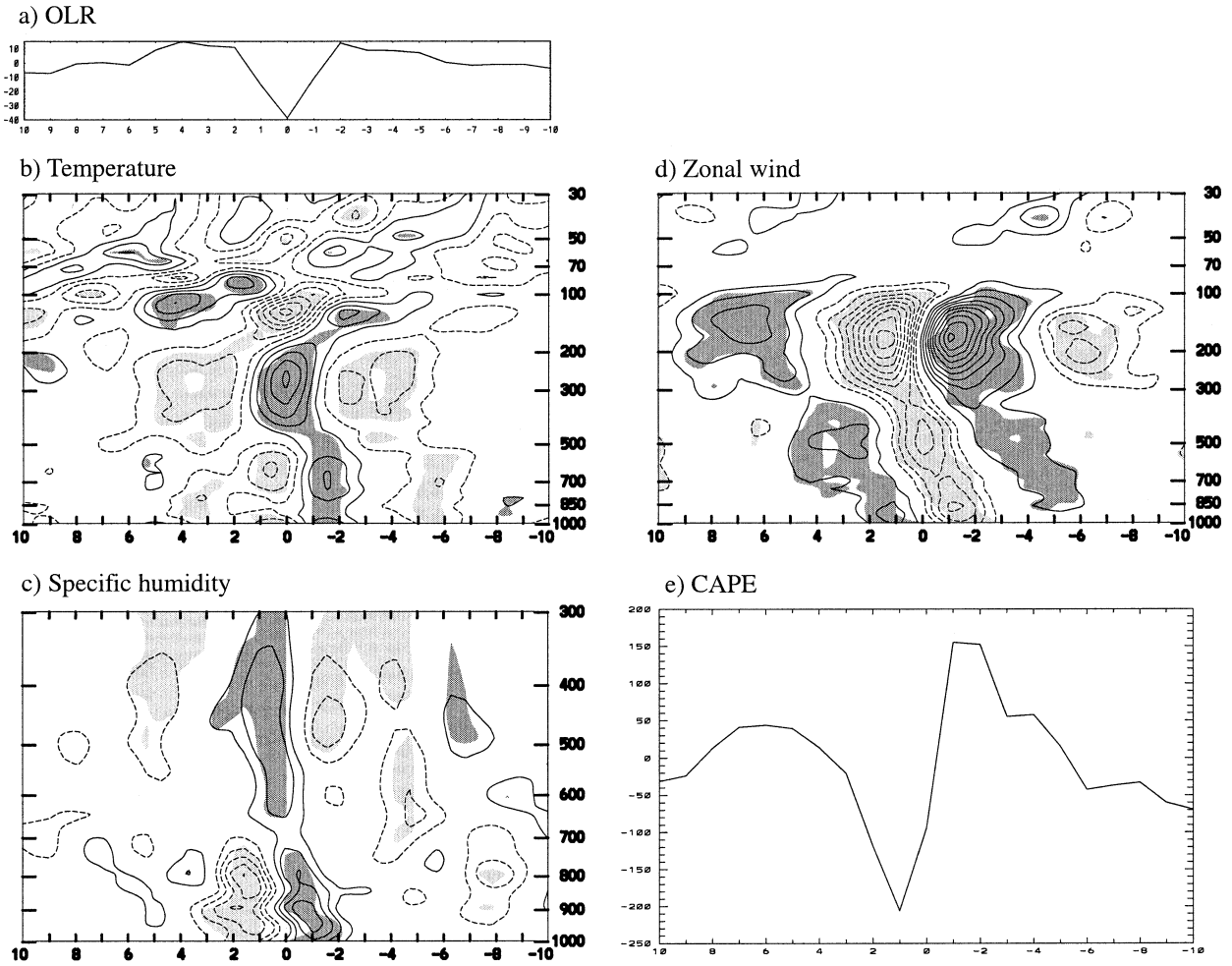

FIG. 5. Regressed (a) OLR, and time–height plots of radiosonde (b) temperature (contour interval 0.1 K), (c) specific humidity (contour interval 0.1 g kg^{-1}; shown only to 300 hPa), (d) zonal wind (contour interval 0.5 m s^{-1}), and (e) time evolution of CAPE at Majuro (7.1°N, 171.4°E), based on a -40 W m^{-2} anomaly in Kelvin-filtered OLR at the closest grid point (7.5°N, 172.5°E) on day 0. Time progresses from right to left, so that time–height structures in (b) and (c) can be compared with longitude–height structures in Figs. 3a and 3b. Twenty-seven levels of data are represented in (b) and (d), and 15 levels in (c). Shading represents regions of statistical significance at the 95% level or greater, with dark shading representing positive correlations.

et al. 2000). An analysis of radiosonde data from multiple stations in Indonesia and the Pacific (see section 4d for an example), as well as Central America and Africa, confirms this difference between Kelvin waves in the Indian Ocean and other tropical regions, with the results in the central Pacific being representative of most tropical locations. These contrasting results may be related to differences in the basic-state environments and are a worthy topic of future research.

In the lower troposphere, between about 500 and 850 hPa, temperature and vertical motion anomalies in the Kelvin wave exhibit a near-quadrature relationship, quite different from the in-phase relationship in the upper troposphere. As shown in Fig. 4b, downward motion anomalies at 700 hPa (light shading) lead warm temperatures (solid contours), which lead upward motion (dark shading) and cold temperatures (dashed contours).

d. Radiosonde comparisons

A similar regression technique was applied to radiosonde data from Majuro, Marshall Islands (7.1°N, 171.4°E), to determine the local temperature, humidity, and wind changes associated with the passage of a Kelvin wave OLR signal. Figures 5a–d show the regressed OLR, temperature, specific humidity, and zonal wind anomalies associated with a -40 W m^{-2} anomaly in Kelvin wave–filtered OLR at the closest grid point to Majuro (7.5°N, 172.5°E) on day 0, plotted from day -10 to day $+10$. A primarily second baroclinic mode temperature structure can be seen in the troposphere (Fig. 5b), as in the reanalysis regressions, with a strong warm anomaly in the upper troposphere peaking on day 0, coincident with the lowest OLR. A warm anomaly in the lower troposphere, centered at 700 hPa, precedes

the low OLR, maximizing between days −2 and −1, while a lower-tropospheric cold anomaly follows the low OLR, with a peak between days +1 and +2. These signals extend to the surface with no apparent change in phase, in contrast to the reanalysis data in Fig. 3a, where surface temperature anomalies lag those in the lower troposphere. The difference in the structure of the lower-tropospheric temperature anomalies in the reanalysis and radiosonde regressions suggests that the shallow convective heating in the reanalysis may be too strong. Overall, however, the ECMWF reanalysis does appear to successfully resolve the vertical temperature structure of convectively coupled Kelvin waves.

Evidence of the effects of shallow convection, deep convection, and stratiform precipitation can be seen in the time–height diagram of regressed specific humidity at Majuro in Fig. 5c. Prior to the lowest OLR on day 0, there is a rapid increase in lower-tropospheric moisture, with moist anomalies maximizing between approximately 850 and 950 hPa on day −1. The significant depth of the moisture increase, to 700 hPa, suggests that shallow convection plays a role in transporting moisture upward. On day 0, when deep convection occurs at Majuro, positive specific humidity anomalies extend through the troposphere to 300 hPa, suggesting the vertical transport of moisture by deep convection. There is an abrupt change from moist to dry air below 700 hPa on day 0, while moist anomalies linger in the upper troposphere for several more days. The moist over dry anomalies observed on days +1 and +2 suggest the presence of both deep convection and stratiform precipitation. The radiosonde humidity signals in Fig. 5c are consistent with those in the reanalysis regressions in Fig. 3b, where enhanced lower-tropospheric moisture exists to the east of the low OLR, and enhanced upper-tropospheric moisture maximizes between 400 and 500 hPa to the west of the low OLR.

Figure 5d shows the regressed zonal wind anomalies at Majuro. Surface easterlies precede the deep convection, maximizing between days −2 and −1, and westerlies follow, maximizing on day +1. Surface zonal wind convergence can be estimated from the zonal wind gradient to be strongest between days −1 and 0, peaking before the lowest OLR signal in a similar manner to the reanalysis regression (not shown). Between 300 and 100 hPa, strong westerly anomalies change to easterly anomalies on day 0, signaling a maximum in divergent outflow occurring in phase with deep convection in the Kelvin wave, also similar to the reanalysis regression (not shown).

The regressed 1000-hPa convective available potential energy anomalies at Majuro are shown in Fig. 5e. CAPE is defined as the net positive area on a thermodynamic diagram, between the observed temperature sounding and the temperature of a parcel lifted moist pseudoadiabatically from the lifting condensation level to the level of neutral buoyancy (Emanuel 1994). The mean CAPE at Majuro for the 21-yr JJA period is 2154 J kg^{-1}. CAPE peaks on days −2 and −1, when the surface air is anomalously warm and moist and the upper troposphere is cool. A sharp decline in CAPE occurs between days −1 and +1, as the convective and stratiform cloud systems within the Kelvin wave envelope dry and cool the lower troposphere and moisten and warm the upper troposphere, as was also observed by Sherwood and Wahrlich (1999). Similar regressions were calculated based on CAPE datasets constructed by holding either temperature or moisture anomalies fixed to their climatological JJA values, as in Cripe and Randall (2001). Results indicate that moisture fluctuations account for the vast majority of the CAPE signal associated with convectively coupled Kelvin waves.

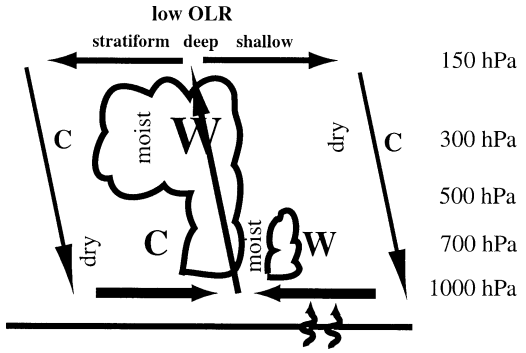

FIG. 6. Schematic diagram of convectively coupled Kelvin wave structure. The letter W (C) represents warm (cold) anomalies. Width of arrows and size of text denotes relative strength of anomalies. Upward arrows crossing the lower boundary represent surface fluxes.

The regressed temperature, moisture, wind, and CAPE anomalies at Majuro are similar to regressions using radiosonde data at other tropical stations (and the corresponding Kelvin-filtered OLR at the nearest grid point to each station), such as Tarawa (central Pacific), Truk (western Pacific), Balboa (Central America), and Bangui-Mpoko (Africa). The similarities between these station data suggest that the Kelvin wave structures illustrated for Majuro are robust, and that the vertical structures and phase relationships in Kelvin waves are not strongly affected by differences in the basic state.

e. Summary

Presented in Fig. 6 is a schematic diagram illustrating the phase relationships in the zonal–vertical plane in observed convectively coupled Kelvin waves. Circulation cells tilt westward with height, such that surface convergence leads upper-tropospheric upward motion by approximately an eighth of a cycle. Surface convergence is in phase with lower-tropospheric upward motion anomalies, and slightly lags lower-tropospheric warm and moist anomalies. Upper-tropospheric upward motion lags that in the lower troposphere, and is in phase with low OLR, warm temperatures, and upper-tropospheric divergence. Upper-tropospheric moisture anomalies lag vertical motion anomalies by about an eighth

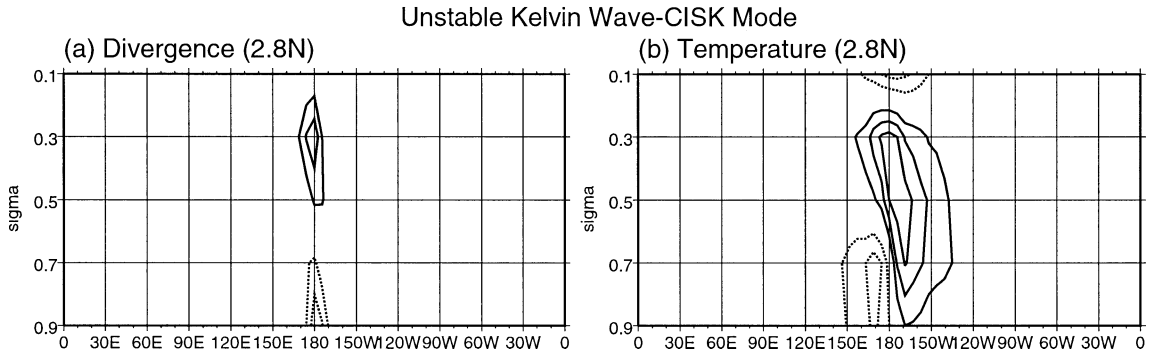

FIG. 7. Structure of unstable Kelvin wave-CISK mode from Matthews and Lander (1999). Longitude–height cross sections at 2.8°N of (a) divergence (contour interval is 1×10^{-6} s^{-1}) and (b) temperature anomaly (contour interval is 0.2 K). Negative contours are dashed and the zero contour is omitted.

of a cycle. The observed tropospheric temperature structure projects primarily onto the second baroclinic mode. In the lower troposphere, temperature and vertical motion anomalies are in quadrature, while in the upper troposphere, temperature and vertical motion anomalies are in phase. This schematic diagram is consistent with the modeling results of Raymond and Torres (1998, their Fig. 25). The implications of these phase relationships for the wave-CISK, WISHE, and stratiform instability mechanisms of wave growth are discussed in the following section.

5. Discussion and conclusions

a. Comparisons of observations with coupled wave instability theories

1) WAVE-CISK

As discussed in section 2a, a central feature of wave-CISK theory is an in-phase relationship between heating and temperature, generated when low-level convergence forces convection. This relationship implies that latent heating more than compensates for the adiabatic cooling due to upward motion in a wave. Figure 4a indicates a strong spatial and temporal correlation between warm upper-tropospheric temperatures, upward motion, and low OLR in the reanalysis, and Fig. 5b illustrates an in-phase relationship between low OLR and warm upper-tropospheric temperatures in radiosonde data. Low-level convergence consistently precedes the heating and temperature anomalies by approximately an eighth of a cycle (not shown). These relationships are consistent with the generation of EKE by condensational heating within the wave, as in wave-CISK-type formulations.

In the lower troposphere, the relationship between heating and temperature is less clear. If low OLR is assumed to represent heating throughout the atmospheric column (i.e., a first baroclinic mode heating), then lower-tropospheric warm anomalies lead deep heating by at least a quarter cycle (Figs. 3a and 5b), and there exists a negative correlation between lower-tropospheric temperatures and heating. However, the increase in lower-tropospheric moisture prior to the lowest OLR (Figs. 3b and 5c) suggests the presence of shallow convection leading deep convection. It is difficult, however, to assess the precise lower-tropospheric heating and temperature relationships due to shallow convection without a detailed knowledge of the shallow convective heating fields themselves.

The structure of modeled Kelvin wave-CISK modes can be compared with observed waves to assess the degree to which the modeled waves reproduce observations. Figure 7 illustrates an example of a Kelvin wave-CISK mode from Matthews and Lander (1999). This unstable Kelvin mode was generated in a primitive equation model using a positive-only CISK parameterization scheme, in which convective heating is proportional to low-level convergence. The vertical structure of the heating profile is specified as top heavy, with maximum heating in the mid- to upper troposphere. Surface convergence slightly leads upper-tropospheric divergence in the modeled wave in Fig. 7, in a similar manner to the observed waves. A deep warm anomaly exists ahead of the maximum vertical motion, while a second mode temperature anomaly exists to its west, leading to a positive correlation between heating and upper-tropospheric temperature. Observed Kelvin waves also show a second mode temperature anomaly in phase with the deep convective heating, as well as a weak first mode warm anomaly to the east (see day -1 in Fig. 5b).

The deep warm anomaly ahead of the convective heating in Fig. 7, and the second mode warm over cold anomaly behind it, give the appearance of a westward-tilted temperature anomaly, as noted in observed Kelvin waves in WKW00 and illustrated in Figs. 3a and 5b. The very simple convective parameterization in the Matthews and Lander (1999) model is able to reproduce this westward tilt simply because it assumes a top-heavy heating profile [see also similar model results in Lau and Peng (1987), Chang and Lim (1988), and Lim et al. (1990)]. When convective heating is activated, the top-heavy heating profile separates into its component

vertical modes, including a first baroclinic convective heating and a second baroclinic stratiform heating over cooling (Mapes 1998). The deep warm anomaly ahead of the vertical motion in the modeled wave in Fig. 7 is produced by the faster first baroclinic mode, while the warm over cold anomaly to the west arises from the more slowly propagating second mode. A positive correlation between heating and upper-tropospheric temperature generates the energy required for this instability. The reduced phase speed of 24 m s^{-1} in the unstable Kelvin mode is set by the dry phase speed of the second vertical mode, which produces a stronger convergence anomaly than the first mode and thus more strongly influences the convective heating (Matthews and Lander 1999). Chao (1995) suggests that the maximum wave-CISK instability is produced when the heating travels eastward with a speed close to, but slightly less than, that of the free Kelvin wave.

The two primary vertical modes into which the initial top-heavy heating profile decomposes in the Matthews and Lander (1999) Kelvin wave-CISK model are similar to the two vertical modes in the stratiform instability model of Mapes (2000), as discussed in section 2c. In both models, temperature anomalies associated with unstable waves have westward tilts with height, and the propagation speed is set by the second vertical mode. The simple wave-CISK parameterization implicitly subsumes the effects of stratiform precipitation into the top-heavy vertical heating profile, while Mapes's stratiform instability model explicitly parameterizes the separate convective and stratiform heating processes. The similarity between the simulated waves in these two models and observations suggests that the first two baroclinic modes are of primary importance in controlling the dynamics of convectively coupled Kelvin waves.

2) WISHE

WISHE theory predicts that coupled waves in a strict QE system will be modified such that enhanced surface heat fluxes and warm tropospheric temperatures precede upward motion, leading to a positive correlation between heating and temperature, and thus wave amplification. As illustrated in Fig. 2, surface easterly anomalies to the east of the low-OLR signal are stronger than the westerly anomalies to its west prior to day 0, when the wave is amplifying, whereas westerly anomalies are stronger than easterly anomalies after day 0, when the wave is dissipating. Similarly, radiosonde zonal winds (Fig. 5d) show stronger surface easterly anomalies as the Kelvin wave propagates past. If surface wind speeds are considered to be a good indicator of latent heat flux, these observations provide support for the WISHE mechanism of wave intensification, particularly since the basic-state winds in the Pacific during JJA are easterly. However, observations of Kelvin waves over the Indian Ocean and Africa show consistently stronger westerlies to the west of the convection than easterlies to its east, in both the amplifying and dissipating phases of the wave (see Fig. 4 in WKW00 for the Indian Ocean case). Basic-state winds in these regions are near zero to westerly. In contrast to the results for Kelvin waves in the Pacific, the observations in the Indian Ocean and African regions do not support the WISHE mechanism of instability, although it is certainly likely that surface heat fluxes do play some role in these waves.

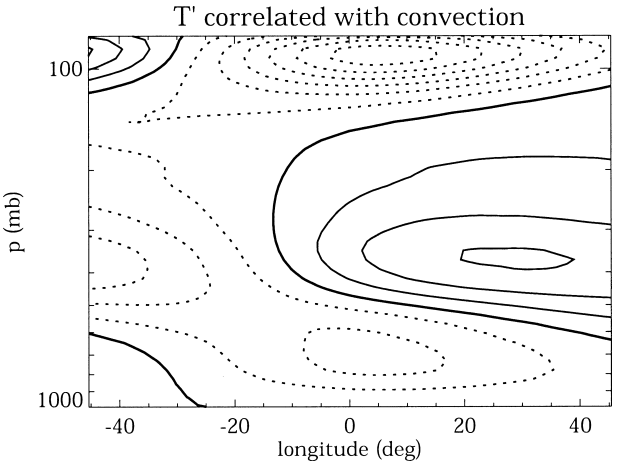

FIG. 8. Structure of stratiform instability mode from Mapes (2000). Longitude–height cross section of regressed temperature (contour interval 0.25 K) based on a +1 std dev anomaly in convection at 0° longitude. Zero contour heavy; negative contours dashed.

3) STRATIFORM INSTABILITY

The primary control on the organization of convection in the stratiform instability model of coupled equatorial waves, as formulated by Mapes (2000), is CIN. A reduction in CIN at the leading edge of a large-scale second baroclinic mode temperature wave allows deep convection to be initiated; convection is then followed at lag by a second mode stratiform heating over cooling profile. The positive feedback between the second mode temperature wave and the second mode heat source provides the energy for wave amplification.

Figure 8 illustrates the regressed temperature structure of the modeled eastward-propagating stratiform instability waves in Mapes (2000), centered on the longitude of maximum convective heating. A second baroclinic mode structure is apparent between 1000 and 200 hPa, which is qualitatively similar to the Kelvin wave observations presented in Fig. 3a. The fact that the stratiform instability model and observations both show strong second baroclinic mode temperature structures suggests that the stratiform heating component is important for the dynamics of these waves (see also Majda and Shefter 2001).

Prior to the convective maximum in the modeled wave, a second mode warm over cold anomaly cools the lower troposphere, reducing CIN. The initial lower-tropospheric cold anomaly reaches a given location ap-

proximately 2 days prior to the convective maximum (given an eastward phase speed of 23 m s^{-1}, with the edge of the cold anomaly located approximately 40° to the east of the convective maximum, as shown in Fig. 8), and increases in intensity until convection maximizes. Observations of Kelvin waves in the Pacific and other locations, however, show a lower-tropospheric warming preceding the deep convection in the wave (Figs. 3a and 5b), and a cooling coincident with and following the deep convective maximum. These observations suggest that a decrease in CIN may not be the driving factor in initiating convection in observed convectively coupled Kelvin waves.

CAPE maximizes in the modeled waves prior to the onset of convection, as also seen in observations (Fig. 5e). While convection is active, CAPE remains low, suggesting that the production of available energy by the large-scale vertical motion and moisture fields is offset by its consumption by convection (i.e., a QE balance). In nonconvective periods, positive CAPE anomalies are regenerated primarily by second vertical mode cold over warm anomalies. This evolution is partially supported by observations that show that the increase in CAPE prior to deep convection is coincident with a warming and moistening at the surface and a cold anomaly aloft (Figs. 5b and 5c).

The phase relationship between heating and upper-tropospheric temperature in the modeled wave in Fig. 8 is significantly different from observations, however. In the modeled wave, the maximum upper-tropospheric warm anomalies lead convection by about 30°, whereas in observations (Fig. 5b), upper-tropospheric warm anomalies are collocated with convection. These differences suggest that temperature anomalies are more strongly influenced by local diabatic processes (i.e., latent heating) in observed Kelvin waves than in the modeled waves.

b. Conclusions

It is important to emphasize here that the three instability theories described in this paper (wave-CISK, WISHE, and stratiform instability) were not originally intended to account for the detailed structures of convectively coupled equatorial waves, but were formulated to explain the fundamental mechanisms of the convective-dynamical instability. The observations presented in section 4 show that aspects of each theory do appear to be relevant to the observed wave structure. The following discussion suggests an evolution of the coupled Kelvin wave that incorporates elements of each of these theories. This discussion is not meant to provide a definitive explanation of the dynamics involved in convectively coupled Kelvin waves, but instead is intended to offer an interpretation of the observations in the context of the three wave intensification theories.

Observations suggest the existence of a Kelvin wave–like circulation prior to coupled wave intensification. WKW00 present evidence of a fast, uncoupled eastward-propagating surface pressure signal preceding the development of a convectively coupled Kelvin wave in the Indian Ocean. SK03 show shallow surgelike features spreading equatorward from the extratropics in association with an upper-tropospheric equatorward-propagating Rossby wave train in the Southern Hemisphere, which develop Kelvin wave characteristics when they reach the equator. These observations suggest that a dry, or uncoupled, Kelvin wave circulation may provide the initial forcing necessary for the development of the coupled wave.

Once a preexisting Kelvin wave circulation has been established in the equatorial region, enhanced surface fluxes may occur within the anomalous low-level easterly flow to the east of the rising branch of the wave. The enhanced surface fluxes may promote the development of shallow convection, which both moistens and warms the lower troposphere. This interaction may provide a positive correlation between lower-tropospheric temperature and shallow convective heating, thus amplifying the lower-tropospheric portion of the wave. Deep convection is initially suppressed by the low CAPE, increased stability, and high CIN that result from the warm and (relatively) dry lower troposphere. CAPE continues to increase throughout this period, however, through the effects of surface fluxes (Parker 2002) and the convergence of moisture forced by the convergent lower-tropospheric winds. As the Kelvin wave circulation propagates eastward, the wave-induced lower-tropospheric warm anomalies are reduced, such that convection gradually increases in vertical extent, initially feeding on the high CAPE and boundary layer moisture remaining from the suppressed phase. Low-level convergence and deep upward motion then provide a continuous source of moisture and instability to fuel deep convection.

Within the large-scale envelope of upward motion, deep convection organizes into larger-scale cloud systems that generate regions of stratiform precipitation, consistent with the stratiform instability mechanism. The combination of the convective and stratiform heating profiles within these numerous mesoscale cloud systems produces a large-scale top-heavy distribution. A QE-like state is maintained, with small but significant departures from exact thermodynamic balance evident in the upper- (lower-) tropospheric warm (cold) anomalies. The coexistence of these primarily second baroclinic mode temperature anomalies and the top-heavy heating profile provides a positive correlation between temperature and heating in the upper troposphere, in a manner consistent with both the wave-CISK and stratiform instability mechanisms. The westward tilt with height of the temperature anomalies results from a combination of the shallow convective heating and/or dry Kelvin wave structure in the lower troposphere to the east of the deep convection, and the top-heavy heating profile in the region of deep ascent in the wave. Since

heating and warm temperature anomalies are in phase in the upper troposphere as well as the lower troposphere, the coupled wave grows in amplitude.

A recent study by Wu (2003) presents a ''shallow CISK, deep equilibrium'' mechanism for convective coupling that may provide another simple model with which to compare observations in the future. In the shallow CISK, deep equilibrium framework, shallow convection initially converges boundary layer moisture, and the low-level circulation intensifies through a CISK-like mechanism. The combination of in-cloud heating and a strong cloud-top cooling slowly erodes any preexisting inversion layer, such that deep convection is then able to penetrate through to the upper troposphere. Since the circulations associated with deep heating propagate away much faster than those associated with shallow heating, the deep modes radiate away and the shallow convection controls the phase speed of the wave. The evolution of this wave appears to be very similar to observations, with shallow convection preceding deep heating and a vertical structure determined by both the shallow and deep modes.

The observations and discussions presented in this paper are intended to motivate future modeling studies of convectively coupled equatorial waves. Successful simulations of these coupled modes will undoubtedly provide additional insights into the fundamental relationships between convection and the large-scale circulation in the Tropics.

Acknowledgments. We thank David Randall, Zhaohua Wu, Jun-Ichi Yano, and one anonymous reviewer for their comments on earlier versions of this paper. The OLR and ECMWF reanalysis data used in this study were obtained from the NOAA–CIRES Climate Diagnostics Center. This work was supported by the Pan American Climate Studies Program of the NOAA Office of Global Programs under project GC98-627.

REFERENCES

Andrews, D. G., J. R. Holton, and C. B. Leovy, 1987: *Middle Atmospheric Dynamics.* International Geophysics Series, Vol. 40, Academic Press, 489 pp.

Arakawa, A., and W. H. Schubert, 1974: Interaction of a cumulus cloud ensemble with the large-scale environment, Part I. *J. Atmos. Sci.,* **31,** 674–701.

Chang, C.-P., and H. Lim, 1988: Kelvin wave-CISK: A possible mechanism for the 30–50 day oscillations. *J. Atmos. Sci.,* **45,** 1709–1720.

Chao, W. C., 1995: A critique of wave-CISK as an explanation for the 40–50 day tropical intraseasonal oscillation. *J. Meteor. Soc. Japan,* **73,** 677–684.

Cripe, D. G., and D. A. Randall, 2001: Joint variations of temperature and water vapor over the midlatitude continents. *Geophys. Res. Lett.,* **28,** 2613–2616.

Crum, F. X., and T. J. Dunkerton, 1992: Analytic and numerical models of wave-CISK with conditional heating. *J. Atmos. Sci.,* **49,** 1693–1708.

Emanuel, K. A., 1987: An air–sea interaction model of intraseasonal oscillations in the Tropics. *J. Atmos. Sci.,* **44,** 2324–2340.

——, 1994: *Atmospheric Convection.* Oxford University Press, 580 pp.

——, J. D. Neelin, and C. S. Bretherton, 1994: On large-scale circulations in convecting atmospheres. *Quart. J. Roy. Meteor. Soc.,* **120,** 1111–1143.

Haertel, P. T., and R. H. Johnson, 1998: Two-day disturbances in the equatorial western Pacific. *Quart. J. Roy. Meteor. Soc.,* **124,** 615–636.

Hayashi, Y.-Y., 1970: A theory of large-scale equatorial waves generated by condensation heat and accelerating the zonal wind. *J. Meteor. Soc. Japan,* **48,** 140–160.

Hendon, H. H., and M. L. Salby, 1994: The life cycle of the Madden–Julian Oscillation. *J. Atmos. Sci.,* **51,** 2225–2237.

Houze, R. A., 1997: Stratiform precipitation in regions of convection: A meteorological paradox? *Bull. Amer. Meteor. Soc.,* **78,** 2179–2196.

Lau, K.-M., and L. Peng, 1987: Origin of low-frequency (intraseasonal) oscillations in the tropical atmosphere. Part I: Basic theory. *J. Atmos. Sci.,* **44,** 950–972.

Liebmann, B., and C. A. Smith, 1996: Description of a complete (interpolated) outgoing longwave radiation dataset. *Bull. Amer. Meteor. Soc.,* **77,** 1275–1277.

Lim, H., T.-K. Lim, and C.-P. Chang, 1990: Reexamination of wave-CISK theory: Existence and properties of nonlinear wave-CISK modes. *J. Atmos. Sci.,* **47,** 3078–3091.

Lin, X., and R. H. Johnson, 1996: Kinematic and thermodynamic characteristics of the flow over the western Pacific warm pool during TOGA COARE. *J. Atmos. Sci.,* **53,** 695–715.

Lindzen, R. S., 1974: Wave-CISK in the Tropics. *J. Atmos. Sci.,* **31,** 156–179.

Madden, R. A., and P. R. Julian, 1994: Observations of the 40–50-day tropical oscillation—A review. *Mon. Wea. Rev.,* **122,** 814–837.

Majda, A. J., and M. G. Shefter, 2001: Models for stratiform instability and convectively coupled waves. *J. Atmos. Sci.,* **58,** 1567–1584.

Mapes, B. E., 1993: Gregarious tropical convection. *J. Atmos. Sci.,* **50,** 2026–2037.

——, 1998: The large-scale part of tropical mesoscale convective system circulations: A linear vertical spectral band model. *J. Meteor. Soc. Japan,* **76,** 29–54.

——, 2000: Convective inhibition, subgrid-scale triggering energy, and stratiform instability in a toy tropical wave model. *J. Atmos. Sci.,* **57,** 1515–1535.

Matsuno, T., 1966: Quasi-geostrophic motions in the equatorial area. *J. Meteor. Soc. Japan,* **44,** 25–43.

Matthews, A. J., and J. Lander, 1999: Physical and numerical contributions to the structure of Kelvin wave-CISK modes in a spectral transform model. *J. Atmos. Sci.,* **56,** 4050–4058.

Neelin, J. D., and I. M. Held, 1987: Modeling tropical convergence based on the moist static energy budget. *Mon. Wea. Rev.,* **115,** 3–12.

——, ——, and K. H. Cook, 1987: Evaporation–wind feedback and low-frequency variability in the tropical atmosphere. *J. Atmos. Sci.,* **44,** 2341–2348.

Parker, D. J., 2002: The response of CAPE and CIN to tropospheric thermal variations. *Quart. J. Roy. Meteor. Soc.,* **128,** 119–130.

Pires, P., J.-L. Redelsperger, and J.-P. Lafore, 1997: Equatorial atmospheric waves and their association to convection. *Mon. Wea. Rev.,* **125,** 1167–1184.

Raymond, D. J., and D. J. Torres, 1998: Fundamental moist modes of the equatorial troposphere. *J. Atmos. Sci.,* **55,** 1771–1790.

Reed, R. J., and E. E. Recker, 1971: Structure and properties of synoptic-scale wave disturbances in the equatorial western Pacific. *J. Atmos. Sci.,* **28,** 1117–1133.

Rickenbach, T. M., and S. A. Rutledge, 1998: Convection in TOGA COARE: Horizontal scale, morphology, and rainfall production. *J. Atmos. Sci.,* **55,** 2715–2729.

Sherwood, S. C., and R. Wahrlich, 1999: Observed evolution of trop-

ical deep convective events and their environment. *Mon. Wea. Rev.,* **127,** 1777–1795.
Stevens, B., D. A. Randall, X. Lin, and M. T. Montgomery, 1997: Comments on 'On large-scale circulations in convecting atmospheres' by Kerry A. Emanuel, J. David Neelin and Christopher S. Bretherton. *Quart. J. Roy. Meteor. Soc.,* **123,** 1771–1778.
Straub, K. H., and G. N. Kiladis, 2002: Observations of a convectively coupled Kelvin wave in the eastern Pacific ITCZ. *J. Atmos. Sci.,* **59,** 30–53.
——, ——, 2003: Extratropical forcing of convectively coupled Kelvin waves during austral winter. *J. Atmos. Sci.,* **60,** 526–543.
Takayabu, Y. N., 1994: Large-scale cloud disturbances associated with equatorial waves. Part I: Spectral features of the cloud disturbances. *J. Meteor. Soc. Japan,* **72,** 433–448.
Wang, B., 1988: Dynamics of tropical low-frequency waves: An analysis of the moist Kelvin wave. *J. Atmos. Sci.,* **45,** 2051–2065.
Wheeler, M., and G. N. Kiladis, 1999: Convectively coupled equatorial waves: Analysis of clouds and temperature in the wavenumber–frequency domain. *J. Atmos. Sci.,* **56,** 374–399.
——, ——, and P. J. Webster, 2000: Large-scale dynamical fields associated with convectively coupled equatorial waves. *J. Atmos. Sci.,* **57,** 613–640.
Wu, Z., 2003: A shallow CISK, deep equilibrium mechanism for the interaction between large-scale convection and large-scale circulations in the Tropics. *J. Atmos. Sci.* **60,** 377–392.
Xu, K.-M., and D. A. Randall, 2001: Explicit simulation of cumulus ensembles with the GATE phase III data: Budgets of a composite easterly wave. *Quart. J. Roy. Meteor. Soc.,* **127,** 1571–1591.
Yanai, M., S. Esbensen, and J. Chu, 1973: Determination of bulk properties of tropical cloud clusters from large-scale heat and moisture budgets. *J. Atmos. Sci.,* **30,** 611–627.
——, B. Chen, and W.-W. Tung, 2000: The Madden–Julian oscillation observed during the TOGA COARE IOP: Global view. *J. Atmos. Sci.,* **57,** 2374–2396.
Yano, J.-I., and K. Emanuel, 1991: An improved model of the equatorial troposphere and its coupling with the stratosphere. *J. Atmos. Sci.,* **48,** 377–389.